



Ionic conductivity enhancement of PVA: carboxymethyl cellulose poly-blend electrolyte films through the doping of NaI salt

Vipin Cyriac · Ismayil · I. M. Noor ·
Kuldeep Mishra · Chetan Chavan ·
Rajashekhar F. Bhajantri · Saraswati P. Masti

Received: 24 July 2021 / Accepted: 10 February 2022 / Published online: 7 March 2022
© The Author(s) 2022

Abstract In this paper, we report the effect of doping sodium iodide (NaI) salt into a polymer blend matrix of sodium carboxymethyl cellulose (NaCMC) and poly(vinyl alcohol) (PVA). Solution casting approach was used to prepare solid polymer electrolyte (SPE) films. The films were characterized by Fourier-transform infrared spectroscopy (FTIR), X-Ray diffraction (XRD), electrical impedance spectroscopy, thermogravimetric analysis (TGA), and differential scanning calorimetry (DSC). XRD showed that NaI incorporation decreased the crystallinity of NaCMC/PVA-based SPE. FTIR technique confirmed the complexation of salt with polymer matrix due to the formation of the coordination bond between Na^+

and $-\text{OH}$ group and hydrogen bond between I^- and $-\text{CH}$ group. The sample with 30 wt% NaI showed the highest conductivity of $2.52 \times 10^{-3} \text{ S cm}^{-1}$, strongly influenced by the highest charge concentration (n), not its mobility (μ). DSC analysis revealed an increase in glass transition temperature (T_g) with increasing salt content. TGA studies showed a decrease in thermal stability with salt inclusion. The transference number was found to be 0.99 for the highest conducting sample showing the primary charge carriers are ions. The highest conducting sample exhibited a mechanical strength of 15.42 MPa at room temperature, and it has been used to fabricate a battery to evaluate its suitability in energy storage devices.

V. Cyriac
Department of Sciences, Manipal Academy of Higher Education, Manipal, Karnataka 576104, India

V. Cyriac · Ismayil (✉)
Department of Physics, Manipal Institute of Technology, Manipal Academy of Higher Education, Manipal, Karnataka 576104, India
e-mail: ismayil.mit@manipal.edu; ismayil.486@gmail.com

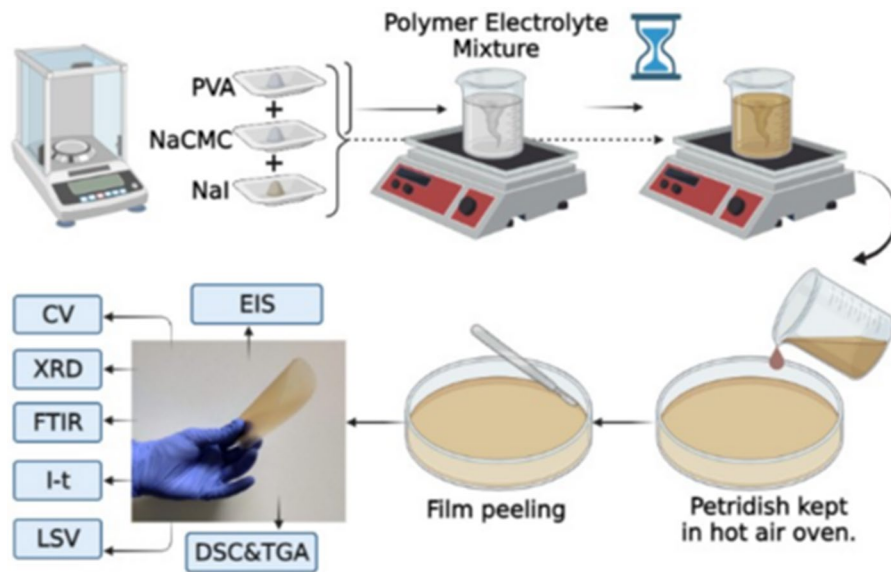
I. M. Noor
Physics Division, Centre of Foundation Studies for Agricultural Science, Universiti Putra Malaysia (UPM), 43400 Serdang, Selangor Darul Ehsan, Malaysia

K. Mishra
Department of Physics, Jaypee University, Anoopshahr, Uttar Pradesh 203390, India

C. Chavan · R. F. Bhajantri
Department of Studies in Physics, Karnataka University, Pavate Nagar, Dharwad, Karnataka 580003, India

S. P. Masti
Department of Chemistry, Karnataka University's Karnataka Science College, Dharwad, Karnataka 580001, India

Graphical abstract



Graphical abstract created with <https://biorender.com>.

Keywords Polymer blend · NaCMC-PVA hybrid · Solid polymer electrolyte · Degree of crystallinity · Ionic conductivity · Transport properties

Introduction

In recent years, researchers have studied polymer electrolytes extensively due to their wide application in batteries, supercapacitors, sensors, solar cells, and fuel cells (Singh et al. 2016). Owing to the low reserves of lithium (Li) sources, the attention has been shifted to sodium-ion batteries (SIBs) based on solid polymer electrolytes (SPEs). They are the best candidate over liquid electrolyte-based lithium-ion batteries (LIBs) since they are economical, has flexible geometry and have no leakage issues. The main advantage is that it uses thin ion-conducting polymer films, significantly reducing its cost and weight (MacGlashan et al. 1999). High ionic conductivity at room temperature ($>10^{-4}$ S cm $^{-1}$), high transference number, wide electrochemical potential window (>4 V), high thermal stability, good mechanical properties, and compatibility with other materials, as well as environmental friendliness, all influence the

performance of solid polymer electrolyte (Jiang et al. 2017). This depends not only on the polymer host where the salt is dissolved but also on the salt doped. Thus, to optimize the desirable properties of a solid-electrolyte to a level of existing commercial liquid electrolyte based LIBs, a fundamental understanding of electrolyte design is required (Li et al. 2005; Fergus 2010; Zhang et al. 2020).

It is critical to strike a balance between energy needs and environmental concerns in the current situation. The use of biopolymers such as starch, cellulose, chitosan, carboxymethyl cellulose (CMC), and gellan gum over the synthetic polymers as a host in electrolytes is exciting due to its excellent film-forming capacity, enhanced safety, abundance, renewability, and environmentally friendly nature (Shetty et al. 2021a).

Many strategies for improving the ionic conductivity of the polymer electrolyte have been applied, including co-polymer grafting, polymer blending, and the use of nanofillers and plasticizers (Ngai et al. 2016). Polymer blending is one of the most viable ones due to its ease of preparation and control of the physical characteristics through the change in composition. In this work, sodium carboxymethyl cellulose

(NaCMC) is the primary component because it has two major functional groups: carboxylate (COO^-) anion and OH group. Poly(vinyl alcohol) (PVA), consisting OH group, will be the second component that can provide multi-point interaction in polymer electrolytes between ionic dopants (Mazuki et al. 2019). PVA also outperforms CMC in terms of mechanical properties. It is highly biocompatible and non-toxic, and thermally and chemically stable. CMC is also highly biodegradable and biocompatible, but it has poor mechanical properties. According to the literature, incorporating CMC into a PVA matrix improves the properties of the CMC counterpart (Khoramabadi et al. 2020).

The literature has shown the complexation of H^+ and Li^+ with CMC/PVA-based blend electrolytes. Mazuki et al. (2018) reported a conductivity of $8.86 \times 10^{-5} \text{ S cm}^{-1}$ for 75.2 wt% CMC-18.8 wt% PVA-6 wt% NH_4Cl . Saadiah et al. (2020) reported 56 wt% CMC-14 wt% PVA-30wt% NH_4NO_3 with the highest conductivity of $1.70 \times 10^{-3} \text{ S cm}^{-1}$. Mohd Ali et al. (2020) reported room-temperature conductivity of $3.92 \times 10^{-3} \text{ S cm}^{-1}$ for 56 wt% CMC-14 wt% PVA-30 wt% NH_4NO_3 plasticized with 6 wt% ethylene carbonate (EC) and $3.00 \times 10^{-3} \text{ S cm}^{-1}$ for the same blend plasticized with 8 wt% polyethylene glycol (PEG). Zulkifli et al. (2020) obtained a maximum conductivity of $3.54 \times 10^{-3} \text{ S cm}^{-1}$ for 64 wt% CMC-16 wt% PVA-20 wt% LiNO_3 system. In all the above work, the most miscible CMC/PVA blend ratio was taken in the weight ratio 80 wt% CMC-20 wt% PVA. Shetty et al. (2021b) reported a conductivity of $5.54 \times 10^{-4} \text{ S cm}^{-1}$ for 56 wt% PVA-24 wt% NaCMC-20 wt% NaBr. But the blend ratio reported (70 wt% PVA-30 wt% NaCMC) is not the most miscible one. Moreover, NaI salt has been extensively studied as the dopant in solid polymer electrolytes (Rani et al. 2014a; Kumar et al. 2014; Saminatha Kumaran et al. 2018; Saidi et al. 2019; Bharati et al. 2020, 2021; Singh et al. 2020; Aziz et al. 2020; Abdullah et al. 2021). However, there is no report of NaCMC/PVA polymer blend with NaI. Therefore, our work focuses on developing solid polymer electrolyte (SPE) films based on the NaCMC/PVA blend with high ionic conductivity and mechanical strength.

Table 1 Designation and sample composition of NaCMC/PVA-NaI SPE system

Sample designation	NaI (wt%)
S0	0
S5	5
S10	10
S15	15
S20	20
S25	25
S30	30

Experimental

Preparation of Solid Polymer Electrolytes (SPEs)

The polymer blend-based solid polymer electrolytes (SPEs) with different NaI salt concentrations are prepared using the solution casting technique. Sodium carboxymethyl cellulose (NaCMC, average molecular weight of $198,000 \text{ g mol}^{-1}$) and poly(vinyl alcohol) (PVA, average molecular weight of $85,000 \text{ g mol}^{-1}$, degree of hydrolysis 85%) were procured from S. D. Fine-Chem, limited, Mumbai. Sodium iodide (NaI, molecular weight of $149.89 \text{ g mol}^{-1}$) was obtained from Merck Life Science Private Limited. NaCMC and PVA with a weight ratio of 80 wt% NaCMC-20 wt% PVA was placed in the beaker along with NaI salt (sample composition has been tabulated in Table 1). 100 mL of double-distilled water was then added into the beaker to dissolve the mixture. The solution was then stirred for 24 h at 70°C . Due to the lack of homogeneous free-standing film formation, doping was limited to 30 wt%. Next, the homogenous mixture was cast onto a glass Petri dish and allowed for slow evaporation at room condition for 7–10 days, followed by drying in the hot air oven at 60°C . The free-standing films were peeled off from a glass petri dish and placed in a desiccator containing silica gel before being used for characterizations. The average thickness of the samples was determined to be between 100 and 200 μm measured with a Mitutoyo micrometer.

Sample characterizations

The structural characterization was performed by employing X-Ray Diffraction (XRD) (Rigaku

Miniflex 600, 5th Gen) with Cu–K α ($\lambda = 1.54 \text{ \AA}$) radiation, at 2θ angle ranging from 5 to 90° with a rate of 2° per minute. The polymer-salt interaction was confirmed from Attenuated Total Reflectance-Fourier Transform Infrared (ATR-FTIR) spectroscopy (SHIMADZU IRPrestige-21 ATR-FTIR) recorded in the transmittance mode between 400 and 4000 cm^{-1} at room temperature with a resolution of 4 cm^{-1} . The electrical impedance spectroscopy (EIS) has been conducted using a precision Impedance analyzer (Hioki Impedance Analyzer IM3570) by applying an alternating voltage of 10 mV to SSISPEISS (SS is stainless steel) in the frequency range between 40 Hz and 1 MHz at room temperature. The impedance data has been transformed to dielectric format to investigate the dielectric properties of the SPEs through complex permittivity, complex conductivity, and tangent loss. The variation of the surface morphology with NaI loading has been investigated using Zeiss EVO 18 Scanning electron microscope (SEM). Thermal properties of prepared SPEs were evaluated using differential scanning calorimetry (DSC) (SHIMADZU DSC-60 PLUS) and thermogravimetric analysis (TGA) (Hitachi STA7200 TGA-DTA) at a temperature rate of 10 $^{\circ}\text{C min}^{-1}$ under a nitrogen atmosphere. Linear sweep voltammetry (LSV) has been performed to estimate the voltage stability window of SPEs prepared. Cyclic voltammetry (CV) has been carried out to confirm the Na-ion transport in the prepared SPEs (Zive SPI, WonATech Co Ltd).

The ion transference number (t_{ion}) has been evaluated using Wagner's polarization technique by

applying a dc voltage of 0.5 V to SSISPEISS where SS is stainless steel. Finally, the mechanical properties of SPEs were evaluated using a Universal Testing Machine (UTM) with a crosshead speed of 0.1 mm min^{-1} (Dak System Inc. 7200 series). According to ASTM D882 requirements, polymer blend electrolytes in a rectangular form with a gauge length of 50 mm and a gauge width of 25 mm were employed. Finally, the highest conducting sample has been used to construct a battery by sandwiching it between cathode and anode. The anode pellet of diameter 12 mm was made using zinc powder, $\text{ZnSO}_4 \cdot 7\text{H}_2\text{O}$ and graphite powder in the ratio 3:1:1 whereas, the cathode pellet of diameter 12 mm was constructed utilising the PbO_2 , V_2O_5 , highest conducting polymer electrolyte, and graphite in the ratio 8:2:1:0.5. Battery parameters such as open-circuit voltage (OCV) and discharge characteristics were measured as a function of time.

Results and discussion

FTIR Spectroscopic studies

The Na^+ cations dissociated from NaI salts are expected to form coordination bonds with the polar groups of the polymer chain backbone. Therefore, FTIR was performed to confirm the complexation by observing the IR bands. The comparative analysis of the FTIR spectra can be done in the following ways: (1) shifting of peaks, (ii) broadening of peaks, and

Fig. 1 **a** FTIR spectra of NaCMC/PVA-NaI SPE system in the wavenumber region of **a** 4000 and 400 cm^{-1} and **b** 3650 and 2790 cm^{-1} (depicting OH and CH vibration modes)

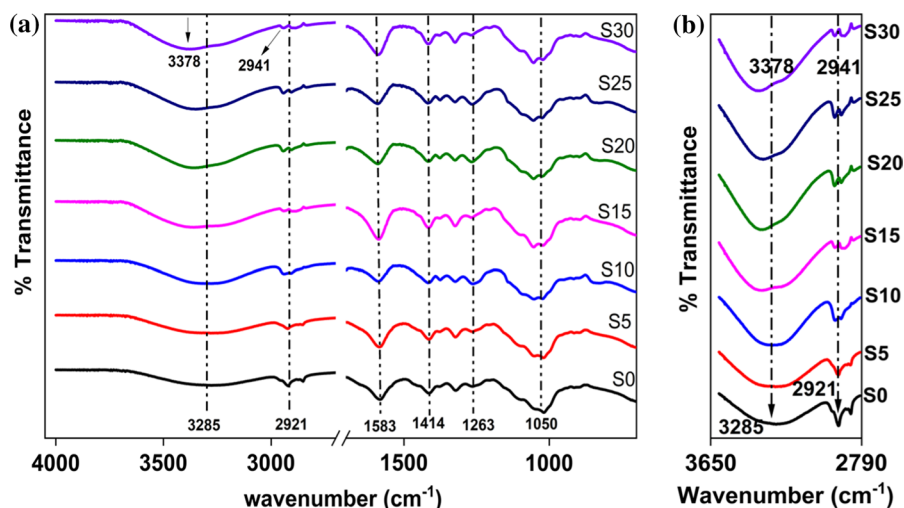


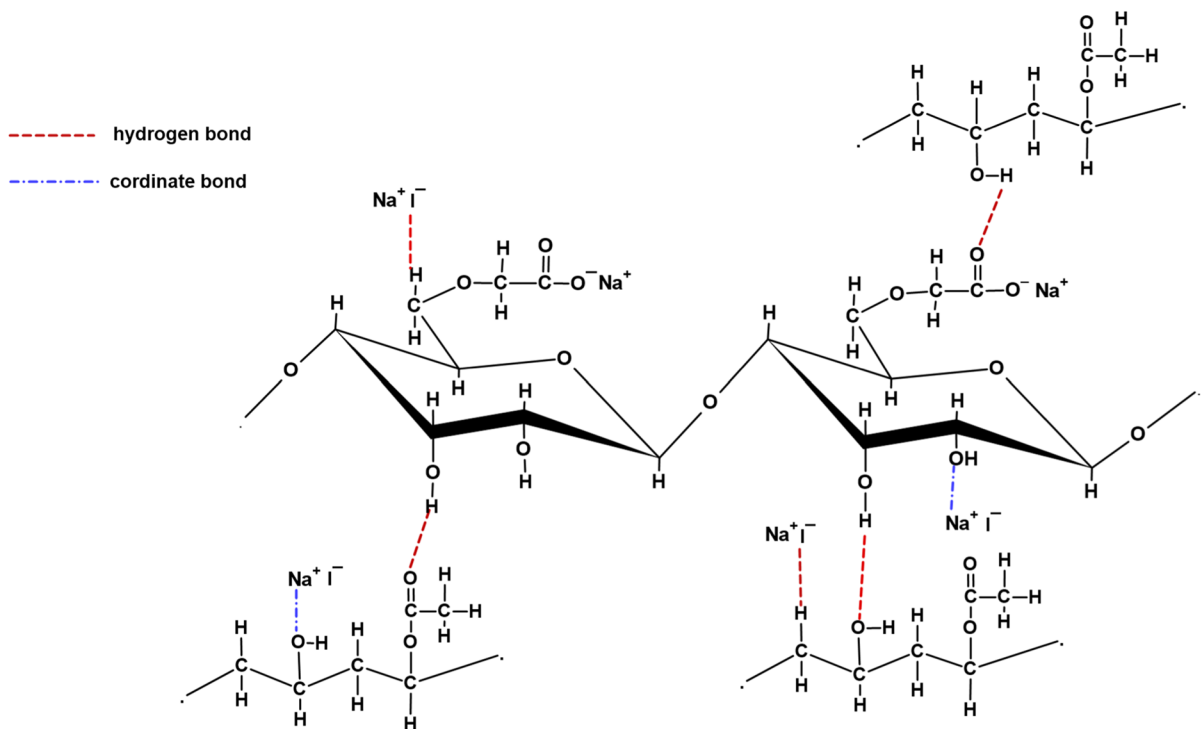
Table 2 Summary of functional groups with the corresponding wavenumber of NaCMC/PVA-NaI SPE system obtained from FTIR

Sample	Functional group with wavenumber (cm^{-1})						
	C–O–C stretching	C–H wagging	O–H bending	C–H ₂ scissoring	COO ⁻ stretching	C–H stretching	O–H stretching
S0	1050	1263	1322	1414	1583	2921	3285
S5	1050	1264	1323	1414	1582	2921	3288
S10	1054	1263	1324	1418	1587	2937	3305
S15	1053	1269	1324	1415	1587	2934	3365
S20	1053	1267	1324	1417	1589	2938	3378
S25	1055	1266	1324	1419	1590	2938	3371
S30	1055	1268	1324	1418	1590	2941	3378

(iii) change in the intensity of specific peaks. Since the moiety attached to the polar group is lighter in our case, the wavenumber shift is expected to occur at the higher wavenumber region (Yadav et al. 2017; Zulkipli et al. 2020). The FTIR spectra for pure NaCMC/PVA blend and blend doped with various NaI salt concentrations are shown in Fig. 1.

Based on the FTIR spectra of the pure NaCMC/PVA blend, seven prominent absorption bands

appears at 1050 cm^{-1} , 1263 cm^{-1} , 1322 cm^{-1} , 1414 cm^{-1} , 1583 cm^{-1} , 2921 cm^{-1} and 3285 cm^{-1} , which correspond to C–O–C stretching, C–H wagging, O–H bending, CH₂ scissoring, COO⁻ stretching, C–H stretching, and O–H stretching, respectively (Ramlli and Isa 2016; Saadiah et al. 2019; Zulkipli et al. 2020). The characteristic of these prominent functional groups at respective wavenumber in

**Fig. 2** Probable interaction scheme of NaI salt with NaCMC/PVA based blend polymer

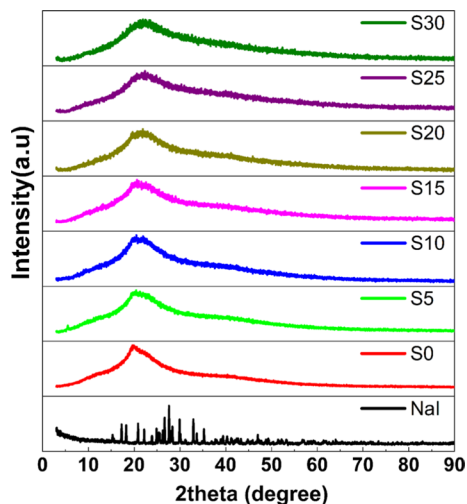


Fig. 3 XRD pattern for NaI salt and NaCMC/PVA-NaI SPE films

the NaCMC/PVA-NaI SPE system are tabulated in Table 2.

From Table 2, it is clearly seen that the wavenumbers corresponding to OH stretching have shifted to a higher wavenumber as well as changed in intensity with an increase in NaI salt concentration (see Fig. 1b). The change in these wavenumbers/intensity variations can be attributed to the cationic coordination of free Na^+ dissociated from NaI salt with the oxygen atom of the OH group via Lewis acid–base interaction. i.e. $\text{Na}^+ \cdots \text{OH}$. Besides, the changes in the wavenumber to the higher side along with changes in intensity corresponding to the $-\text{CH}$ stretching might as well indicate the interaction of the I^- anion of the salt with the H atom of the CH_2 group or with the H atom of the OH group via hydrogen bond i.e. $\text{C}-\text{H} \cdots \text{I}^-$ (Steiner 2002; Selvanathan et al. 2018). Thus, the interaction between the salt and the polymer host has been confirmed. The probable interaction scheme is shown in Fig. 2.

X-Ray Diffraction (XRD)

X-ray diffraction was conducted to understand the structural modification brought about by doping NaI into the NaCMC/PVA blend polymer. Figure 3 shows the XRD pattern for NaI salt and NaCMC/PVA-NaI SPE system.

The XRD spectrum of NaI reveals strong peaks, suggesting that it is highly crystalline. It can be seen that the peaks corresponding to NaI are absent in the SPE pattern indicating that NaI salt has completely dissolved in the polymer matrix. The XRD spectra of the prepared SPEs were analyzed by observing the changes in the peak intensity and peak breadth. The decrease in amorphousness is interpreted using Hodge et al. criteria (Hodge et al. 1996) which shows a relationship between crystallinity and peak intensity. The reduction in the relative intensity and increase in the breadth of the peak around 2θ angle between 5 and 70° indicates the increase of the amorphousness of the SPE on doping with NaI salt. The increase in the amorphousness of samples is due to the breaking and formation of bonds (Zulkifli et al. 2020). The Na^+ and I^- ions can disrupt the intermolecular hydrogen bond between polymer chains due to the electrostatic interaction between the Na^+ and OH functional group of the polymer, thereby disrupting the crystalline phase (Selvanathan et al. 2018; Aziz et al. 2020). Based on Fig. 3, it is seen that S30 is the most amorphous sample.

To ascertain this argument, XRD deconvolution was performed to separate the amorphous and crystalline regions of the XRD diffractogram using Fityk software (Wojdyr et al. 2004). It is reported that the CMC is amorphous and has characteristic peaks at 16.5° , 22.5° , and 34.5° (French 2013; De Melo et al. 2017), whereas PVA is semi-crystalline and has a sharp crystalline peak at 19.6° and relatively low peaks at 11.5° , 22.9° , 28.0° , 32.2° and 40.8° (Abd El-Kader et al. 2004; Noor et al. 2013). Since CMC has been blended with PVA, deconvolution peaks from both components have to be considered. Gaussian function was chosen to fit all the XRD diffractograms, and the results are shown in Fig. 4. Baseline correction was applied before the deconvolution process. Since NaCMC-PVA poly-blend (salt-free) films and salt-doped electrolyte films are free-standing films, the sample holder was not used to place the film for the measurement process. Two-point linear background subtraction method has been used to make baseline corrections (Yao et al. 2020). The XRD pattern of the sample was subtracted with the sample-free XRD diffractograms of the instrument. With this, a pure XRD pattern of the sample is obtained. From Fig. 4, it can be seen that two/three amorphous peaks and three crystalline peaks have perfectly fit the

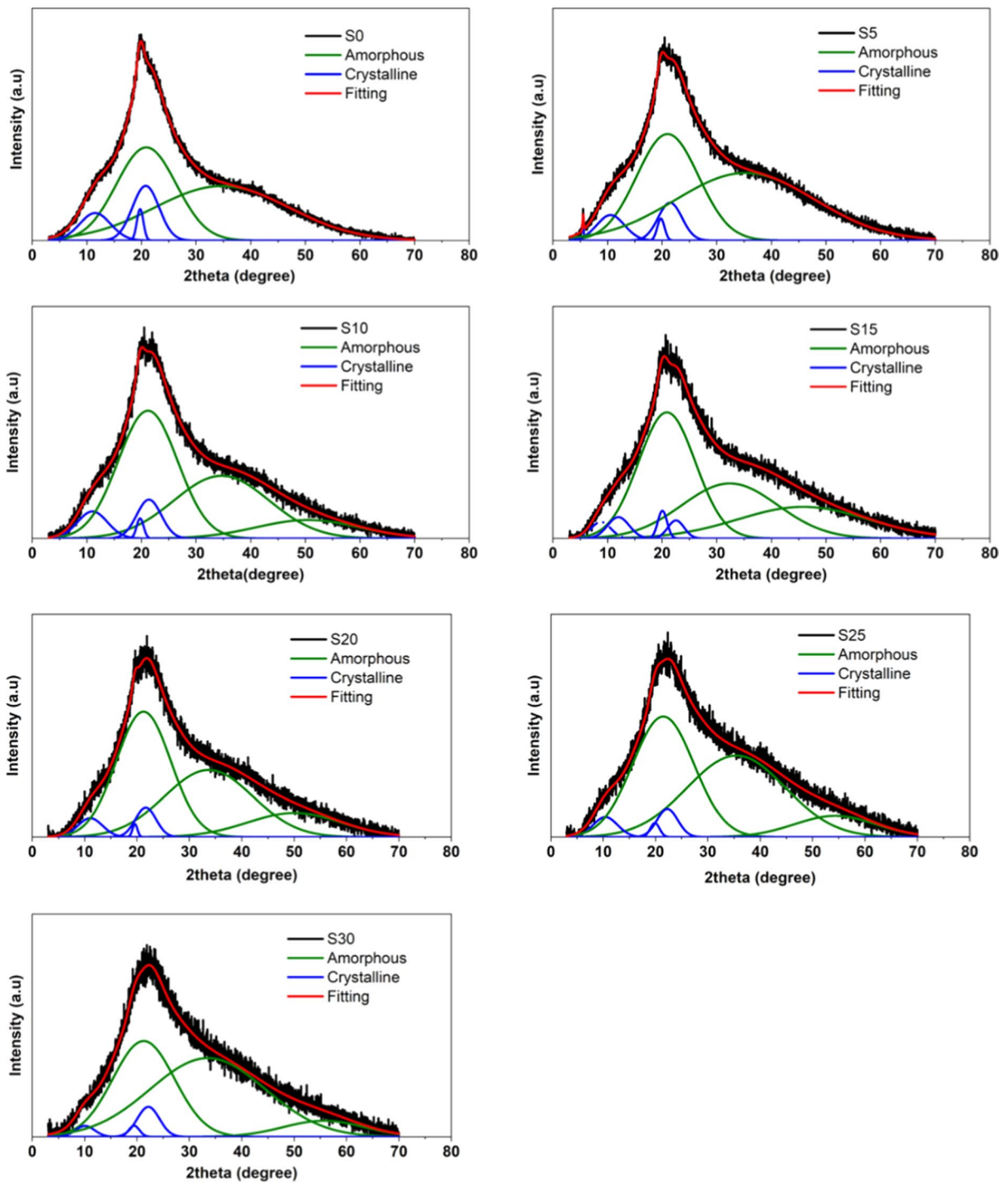


Fig. 4 XRD deconvolution between 2θ angle of 5° and 70° for NaCMC/PVA based SPEs with different NaI salt concentrations

Table 3 Degree of crystallinity for NaCMC/PVA-NaI SPE system

Sample	A_C	A_A	χ (%)
S0	6201.72	31,714.80	16.35
S5	2650.60	23,587.55	10.10
S10	2261.56	18,383.13	10.95
S15	1330.41	16,390.35	7.50
S20	981.77	12,920.36	7.06
S25	911.62	12,871.33	6.61
S30	701.64	11,406.31	5.79

sample's XRD diffractogram. The deconvoluted XRD peaks have been assigned respectively to CMC and PVA components. From the analysis, the degree of crystallinity χ for each sample was calculated using the Eq. (1).

$$\chi = \frac{A_C}{A_C + A_A} \times 100\% \quad (1)$$

Here A_C is the total area under the crystalline peaks, and A_A is the total area under the amorphous peaks (del Cerro et al. 2020). The degree of crystallinity (χ) for each sample is listed in Table 3.

It is clear from Table 3 that with the incorporation of 5 wt% NaI salt, the degree of crystallinity of S0 film (salt-free film) decreased from 16.35 to 10.10%. Increasing the amount of NaI salt up to 30 wt% in the blend polymer matrix is observed to reduce further the degree of crystallinity of NaCMC/PVA-based solid polymer electrolyte and reach a minimum of 5.79%. These results confirmed that S30 film is the most amorphous and is expected to give the highest conductivity among the prepared SPEs.

Electrical impedance spectroscopy (EIS)

The ionic conductivity of the pure and doped polymer blend electrolytes was obtained by electrical impedance spectroscopy at room temperature. Each SPE film was placed between two blocking stainless steel electrodes. Figure 11 shows the Nyquist plots for all prepared electrolytes in the log–log scale due to its superiority over the linear scale (Jonscher 1999; Tang et al. 2015). From Fig. 5, it can be seen that there are two arcs, one at the low-frequency region and the other at the high-frequency region.

The low-frequency arc is related to the electrode–electrolyte interface phenomenon, evidencing the capacitive nature. The high-frequency arc gives information on ion conduction in the bulk electrolyte (Careem et al. 2020). It is clear that the length of the low-frequency arc increases with the increase in salt concentration. In contrast, the arc at high-frequency shortens and disappears at S30, indicating the increase in the capacitive nature. The dip in the plot is used to find the bulk electrolyte resistance (minimum in the $-Z_i$). The dip is observed to shift to the higher frequency region, indicating the decrease in the bulk electrolyte resistance. Since the electrodes are ion blocking, at lower frequencies, ions get accumulated alternatively at the electrode–electrolyte interface and hence a double layer is formed. This is represented as a constant phase element CPE2 (low frequency tilted spike in Nyquist plot). Also, when the field is applied, there is a resistance offered to the flow of ions (represented as R_b) in the bulk and the realignment of dipoles in bulk (represented as another constant phase element CPE1). Since these two phenomena happen simultaneously, a parallel combination of R_b and CPE1 (high frequency depressed semicircle in the Nyquist plot). Thus, the equivalent circuit for S0–S25 consist of CPE1 in series with a parallel combination of R_b and CPE2. The Nyquist plot of the S30 sample was fitted with an equivalent circuit model consisting of a resistor connected in series with a constant phase element (CPE1) since it shows only a tilted spike shape on the Nyquist plot. The Nyquist plots for samples S0 to S30 were fitted with EIS spectrum analyzer software (Bondarenko 2005), with the percentage error in fitting being within 5%. The ionic conductivity of each electrolyte is obtained using the relation of

$$\sigma = \frac{t}{AR_b} \quad (2)$$

where t , R_b , and A is the electrolyte thickness, electrolyte bulk resistance, and contact area of the electrode/electrolyte, respectively. The conductivity for each sample is shown in Table 5. It is found that S30 has the highest conductivity of 2.52×10^{-3} S cm^{-1} , which may be due to the higher charge carrier density and increased amorphousness of the sample, as indicated in the XRD studies. Noor et al. (2013) reported that the conductivity occurs mainly in the amorphous region of the polymer electrolyte.

Polymer electrolytes with high amorphous properties are softer, thus assisting ions to move easily from one coordination site to another under the applied electric field. As a large charger carrier in the sample results from salt dissociation, the movement of ions from one coordination site to another will actively occur. Hence, high ionic conductivity will be obtained. This is in line with what was observed for sample S30, which has the highest conductivity and highest amorphous characteristic.

Figure 6 shows the plot logarithm of ionic conductivity versus $1000/T$ for various salt concentrations for the NaCMC/PVA poly-blend system. The plot is linear, suggesting that the ion conduction behaviour is thermally activated and follow the Arrhenius model. According to this model, temperature-dependent ionic conductivity is given by

$$\sigma(T) = \sigma_0 \exp\left(-\frac{E_a}{k_B T}\right) \quad (3)$$

where σ_0 is a pre-exponential factor, E_a is the activation energy, k_B is Boltzmann constant and T is the absolute temperature. The increase in the conductivity with the temperature can be interpreted as the hopping mechanism between the coordinating sites. The contribution of polymeric chain movements cannot be ignored in the Arrhenius model (Baskaran et al. 2004). This is because, with the increase in temperature, the vibrational motion of the sidechains/polymer backbone brings the coordinate sites together, making the ion hopping with lesser energy (Pawlicka et al. 2008). The values of the activation energy E_a (in eV) is tabulated in Table 4. The activation energy drops with salt concentration and is minimum for the highest conducting sample S30. The dominance of amorphous phase at higher salt concentration facilitates for ionic motion in the polymer electrolyte and thus, lower activation energy (Muthuvinayagam and Gopinathan 2015).

AC conductivity study

All the impedance data obtained from EIS measurements can be transformed into the complex conductivity plot as a function of frequency, as shown in Fig. 7. The complex conductivity is given by

$$\sigma^*(\omega) = \sigma'(\omega) + i\sigma''(\omega) \quad (4)$$

where the real part $\sigma' = \sigma_{ac}$. Two different regions can be seen in the figure: the low-frequency dispersion region and the mid plateau region. Since the ions have enough time to accumulate at the interface at low frequencies, space charge polarization occurs at the electrode/electrolyte interface. The ac conductivity is frequency independent in the plateau region, and extrapolation of this plateau region to the vertical axis (at $\omega \rightarrow 0$) gives dc conductivity (σ_{dc}) (Chitra et al. 2019). It can be seen that with the increase in the salt concentration, the general trend of the shift of the plateau region to the higher frequency region has been observed. Since glass transition temperature (T_g) is above the room temperature as per the DSC, the increase in conductivity is highly attributed to an increase in ion concentration rather than an increase in segmental motion of polymer chain. The bulk conductivity calculated from the Nyquist plot and the DC conductivity estimated from the AC conductivity spectra shown in Table 4 agree well.

Dielectric study

The complex permittivity ϵ^* is represented as $\epsilon^* = \epsilon' - j\epsilon''$, where ϵ' is the real part that associated with the ability of the polymer to dissociate ions and the ϵ'' is the imaginary part that corresponded with the energy required to orient the dipoles and move the ions (Pritam et al. 2020). Figures 8a and b show the variation of ϵ' and ϵ'' as a function of frequency. At low frequencies, both ϵ' and ϵ'' is very high and can be attributed to the electrode polarization effect. At low frequencies, ions have enough time to build up at the electrode/electrolyte interface leading to a very large value of dielectric constant, after that decreases in a non-linear fashion to attain a constant value with increasing frequency. This is because at high frequencies, ions cannot follow the field and cause a sudden decrease. From Fig. 8b, there are no relaxation peaks in the plot of ϵ'' against $\log \omega$ suggesting that the rise in dc conductivity is attributed to an increase in ion density rather than a structural relaxation process related to the reorientation of the dipoles in the system or the segmental relaxation of the polymer chains (Shetty et al. 2021a). It is observed that both ϵ' and ϵ'' increase with salt concentration and is highest for S30 sample. The increase in the dielectric constant

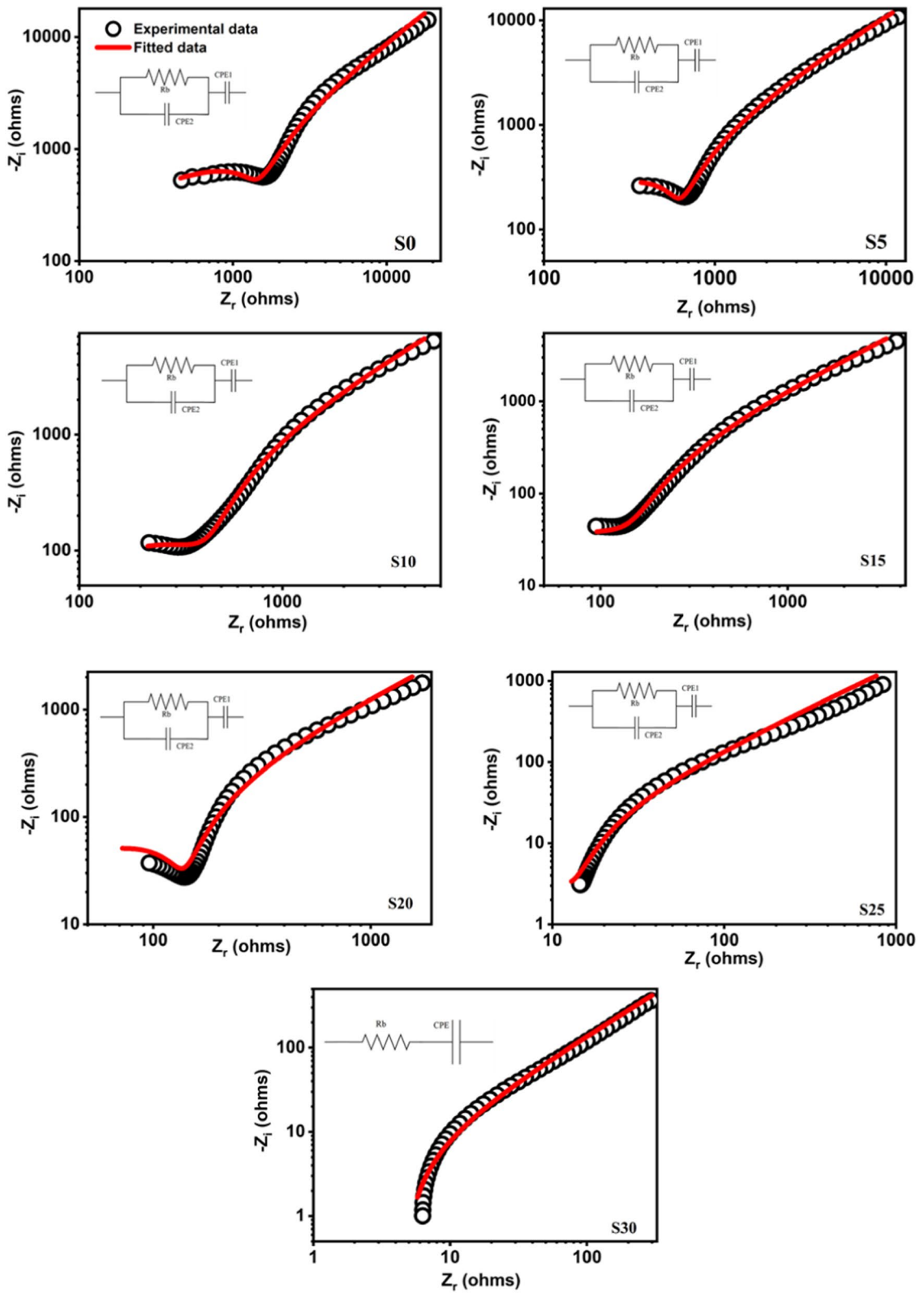


Fig. 5 Nyquist plots for NaCMC/PVA based solid polymer electrolyte with different NaI salt concentrations

can be attributed to the increase in the carrier concentration by the relation

$$n = n_o \exp \left[-\frac{U}{kT\epsilon} \right] \quad (5)$$

where n is the charge carrier concentration, ϵ is the dielectric constant, and U is the salt dissociation energy. This is indeed reflected in the ionic conductivity by the relation $\sigma = \sum_i n_i q_i \mu_i$ (Pritam et al. 2020).

The variation of the tangent loss as a function of frequency is shown in Fig. 8c. The plot consists of a maximum at the characteristic's frequency ω_{max} , indicating the presence of conductivity relaxation. The relaxation time (τ) is calculated using the equation

$$\omega_{max} \tau = 1 \quad (6)$$

In most of the studies (Pritam et al. 2020, 2021), it is observed that the increase in the salt concentration shifted the maximum peak of $\tan \delta$ to a higher frequency range, thereby indicating a decrease in the relaxation time which is generally attributed to the increase in the mobility of ions. But in our work, we do not see such a linear shift in the loss factor peak. This is indeed supported by the anomalous variation in the mobility as suggested in the transport property study (see Sect. 3.6).

Ion transport properties

Parameters like charge carrier density (n), mobility (μ), and diffusion coefficient (D) have been evaluated by fitting the Nyquist plot with the corresponding equivalent circuit model introduced by Arof et al. (2014). The Nyquist plot consists of a depressed semicircle at high frequencies region and tilted spike at low-frequency region is suited to fit using the Eqs. (7) and (8)

$$Z_r = \frac{R + R^2 k_1^{-1} \omega^{p_1} \cos \left(\frac{\pi p_1}{2} \right)}{1 + 2R k_1^{-1} \omega^{p_1} \cos \left(\frac{\pi p_1}{2} \right) + R^2 k_1^{-2} \omega^{2p_1}} + \frac{\cos \left(\frac{\pi p_2}{2} \right)}{k_2^{-1} \omega^{p_2}} \quad (7)$$

$$Z_i = \frac{R^2 k_1^{-1} \omega^{p_1} \sin \left(\frac{\pi p_1}{2} \right)}{1 + 2R k_1^{-1} \omega^{p_1} \cos \left(\frac{\pi p_1}{2} \right) + R^2 k_1^{-2} \omega^{2p_1}} + \frac{\sin \left(\frac{\pi p_2}{2} \right)}{k_2^{-1} \omega^{p_2}} \quad (8)$$

Here R is the bulk resistance, k_1^{-1} , is the geometrical bulk capacitance, k_2^{-1} , is the capacitance of the electric double layer formed at the electrolyte/electrolyte interface, p_1 , is the ratio of the angle between the diameter of the semicircle and vertical axis to the right angle subtended by the real and imaginary impedance axis. p_2 is a skew parameter that controls the degree of the tendency of the tilted spike from the real axis. The values of p_1 and p_2 lie between 0 and 1. For a Nyquist plot consists only a tilted spike shape, Eqs. (9) and (10) are used to fit the complex impedance plot.

$$Z_r = R + \frac{\cos \left(\frac{\pi p}{2} \right)}{k^{-1} \omega^p} \quad (9)$$

$$Z_i = \frac{\sin \left(\frac{\pi p}{2} \right)}{k^{-1} \omega^p} \quad (10)$$

In Eqs. (9) and (10), R is the bulk resistance, k^{-1} and p takes the same character to that of k_2^{-1} and p_2 as in Eqs. (7) and (8). The diffusion coefficient (D), mobility (μ), and number density (n) of charge carriers are estimated with the following equations.

$$D = \frac{e(k_2 \epsilon_r \epsilon_0 A)^2}{\tau_2} \quad (11)$$

$$\mu = \frac{eD}{k_B T} \quad (12)$$

$$n = \frac{\sigma}{\mu e} \quad (13)$$

Here ϵ_r is the dielectric constant at the high-frequency range, k_B is the Boltzmann constant ($1.38 \times 10^{-23} \text{ J K}^{-1}$), T is the absolute temperature, and the value of τ_2 is taken at the frequency corresponding to a minimum in the imaginary parts of the impedance. Table 5 listed the variation of the parameters k_2^{-1} , D , μ and n for NaCMC/PVA-based SPE with different NaI salt concentrations, and the variation is represented in Fig. 9.

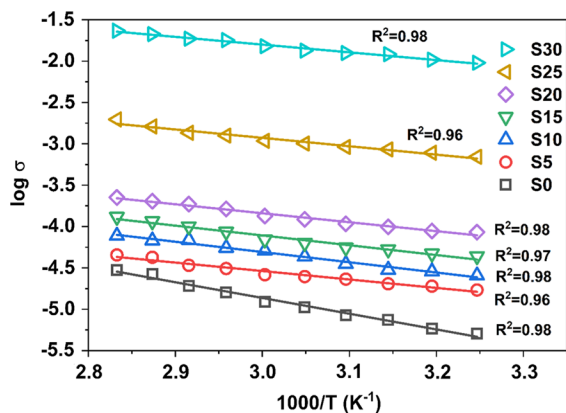


Fig. 6 Arrhenius plot for NaCMC/PVA-NaI polymer blend system (symbols represent the experimental data and the line represent the best-fitted line)

Based on Table 5, it can be seen that the increasing amount of salt concentration in NaCMC/PVA-NaI blend polymer increased the number density of charge carriers. This is because NaI salt dissociated into free Na^+ and I^- ions and formed a complexation with $-\text{OH}$ and $-\text{CH}$ groups of NaCMC/PVA polymer. As more salt is added, more free ion is dissociated resulting in an increase in charge carrier density. Furtado et al. (1999) reported that the incorporation of LiClO_4 up to 22 wt% into a thermoplastic polyurethane-based solid polymer electrolyte reduced the free volume of the sample due to the coordination of Li^+ ions with the polymer polar atom. The free ions concentration increased with increasing LiClO_4 salt concentration up to 22 wt%. A similar trend is observed in this work where the number density of charge carrier increases with increasing NaI salt. This may imply that the free volume of NaCMC/PVA-NaI SPE decreases with the increasing concentration of NaI salt, thus contributing to an increase in electrolyte conductivity. The charge

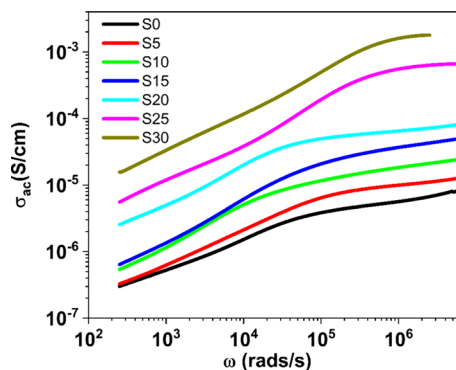


Fig. 7 AC conductivity plots for the NaCMC/PVA based solid polymer electrolyte containing different NaI salt concentration

carrier mobility (μ) and diffusion coefficient (D) is found to be maximum at S15 sample. Later, it is seen to decrease with an increasing salt concentration beyond 15 wt%. The charge carrier density is high at higher salt concentrations, limiting the amount of space available for free ions to move. This phenomenon caused the collision rate to increase, and hence, μ and D decrease (Noor 2020; Chai et al. 2020). It is observed that σ_{dc} and ϵ' follows the same trend from S0 to S30 samples, implying that $\sigma_{dc} \propto n \propto \epsilon'$. Based on the conductivity trend, it can be concluded that the increase in ionic conductivity for NaCMC/PVA-NaI SPE system is strongly influenced by the number density of charge carriers.

Scanning electron microscopy (SEM)

Figure 10 shows the SEM micrographs for NaCMC/PVA-NaI free-standing films at a magnification of 5000x. The S0 film (salt-free) shows smooth morphology without any phase separation, indicating high miscibility between NaCMC and PVA blend

Table 4 Values of bulk resistance (R_b), ionic conductivity (σ), DC conductivity (σ_{dc}), relaxation time (τ) and activation energies (E_a) for NaCMC/PVA-NaI SPE system

Sample	R_b (Ω)	σ (S cm^{-1})	σ_{dc} (S cm^{-1})	τ (s)	E_a (eV)
S0	1115.00	7.95×10^{-6}	6.48×10^{-6}	3.86×10^{-6}	0.377
S5	522.31	1.36×10^{-5}	1.02×10^{-5}	1.72×10^{-6}	0.202
S10	423.87	1.64×10^{-5}	1.94×10^{-5}	1.48×10^{-6}	0.246
S15	148.10	3.91×10^{-5}	4.06×10^{-5}	8.90×10^{-7}	0.234
S20	129.38	7.00×10^{-5}	6.61×10^{-5}	2.00×10^{-6}	0.214
S25	13.29	7.57×10^{-4}	6.07×10^{-4}	1.51×10^{-7}	0.201
S30	4.59	2.52×10^{-3}	1.87×10^{-3}	–	0.185

Fig. 8 Frequency dependency of **a** real permittivity (ϵ') **b** imaginary permittivity (ϵ'') and **c** tangent loss ($\tan \delta$) of NaCMC/PVA based solid polymer electrolyte with different concentrations of NaI

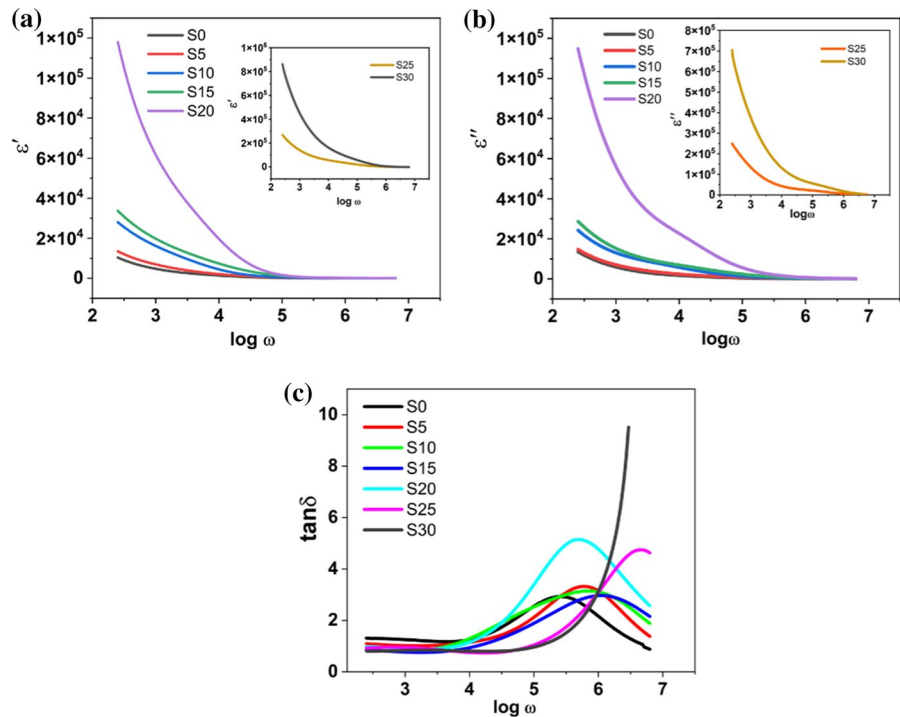


Table 5 Summary of the parameters k_2^{-1} , D , μ and n for NaCMC/PVA-NaI SPE system

Sample	$k_2^{-1}(F)$	$D(\text{cm}^2 \text{s}^{-1})$	$\mu(\text{cm}^2 \text{V}^{-1} \text{s}^{-2})$	$n(\text{cm}^{-3})$
S0	2.81×10^{-6}	3.20×10^{-6}	1.24×10^{-4}	4.00×10^{17}
S5	3.19×10^{-6}	3.14×10^{-7}	1.21×10^{-5}	7.00×10^{18}
S10	4.02×10^{-6}	7.94×10^{-7}	3.07×10^{-5}	3.34×10^{18}
S15	5.57×10^{-6}	2.54×10^{-6}	9.82×10^{-5}	2.49×10^{18}
S20	1.38×10^{-5}	1.60×10^{-7}	6.18×10^{-6}	7.07×10^{19}
S25	2.18×10^{-5}	8.61×10^{-10}	3.33×10^{-8}	1.42×10^{23}
S30	6.74×10^{-5}	6.60×10^{-12}	2.54×10^{-10}	6.18×10^{25}

components. In general, the morphology of the polyblend-salt electrolytes is uniform and homogenous but with a different degree of roughness with the inclusion of NaI salt (Rani et al. 2014b; Tellamekala et al. 2020). With the inclusion of salt, the surface becomes more porous due to the onset of the formation of small but unequal sized pores (free volume). In general, a porous structure is essential for the smooth migration of ions through the polymer structure. These pores enhance Na^+ ion transport by increasing the surface area, which is beneficial for the diffusion

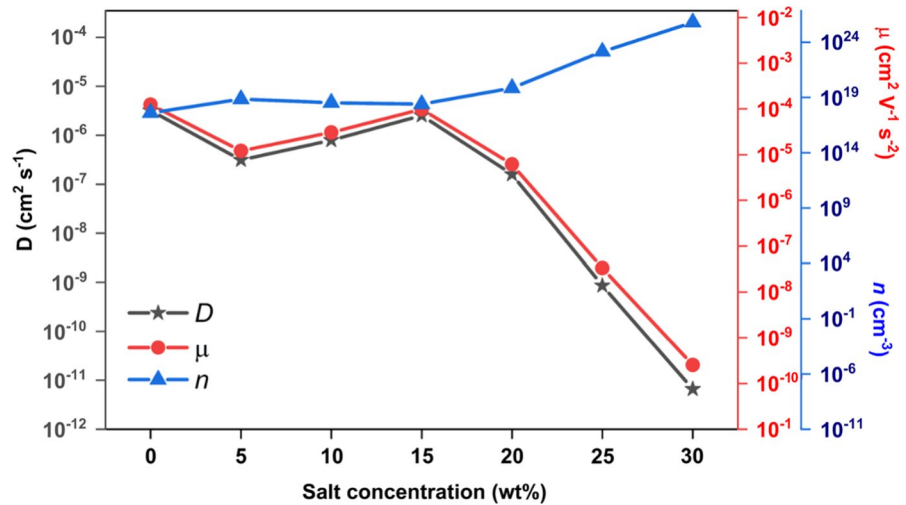
of the ions through the polymer, thereby improving its overall conductivity (Su'ait et al. 2011; Wang et al. 2021). The micro-pores becomes very prominent from S20, and it is very large for S25 and S30 samples; hence mobility and diffusion coefficient are expected to increase. Even though micro-pores are larger in S25 and S30, the diffusion coefficient and mobility are still decreasing as per transport studies since the carrier density is so high that this compensates for the effect of larger pores. Throughout S0 to S30, no salt agglomeration is seen, indicating an agreement with the XRD studies and transport studies where the crystallinity is steadily decreasing and number density is steadily increasing, respectively.

Differential scanning calorimetry (DSC)

The effect of NaI doping in NaCMC/PVA blend polymer on the glass transition temperature (T_g) of SPEs was investigated using DSC. Figure 9 shows the DSC curves of S0 to S30 samples in the temperature range of 27 and 250 °C.

All samples showed a broad endotherm step transition around 50 to 95 °C, which indicates the T_g of the SPEs. Based on the DSC thermogram shown in Fig. 11, a single T_g is observed, indicating the

Fig. 9 Variation of D , μ and n as a function of salt concentration for NaCMC/PVA-NaI SPE system



compatibility of PVA and NaCMC as the blend components (Saadiah et al. 2020). The incorporation of salt has increased the glass transition temperature of the SPEs, which can be attributed to the increased intermolecular interaction between the Na^+ cation and the oxygen atom of the polymer chain. These cross-linkages hinder the polymer chain's rotation, thus increasing the energy barrier. This interaction is exceptionally high for S25 and S30 samples as the charge carrier density are very high, as suggested by the transport analysis, leading to very high T_g in these samples (He and Kyu 2016; Shanmuga Priya et al. 2018). A similar kind of increase in T_g upon incorporating salt into the CMC/PVA blend has been reported earlier, and our study is in-line with these reports (Noor and Isa 2019; Saadiah et al. 2020). According to these studies, the increase in T_g is attributed to the expansion of the polymer chain due to the electrostatic repulsion with the introduction of the charges.

Thermogravimetric analysis (TGA)

In TGA, the mass of the sample is monitored while it is being heated at a constant rate. This causes the bond within the molecule to break, and hence thermal stability of the sample can be studied. TGA thermogram and their first-order derivative curves for S0, S10, S20, and S30 samples are shown in Fig. 12.

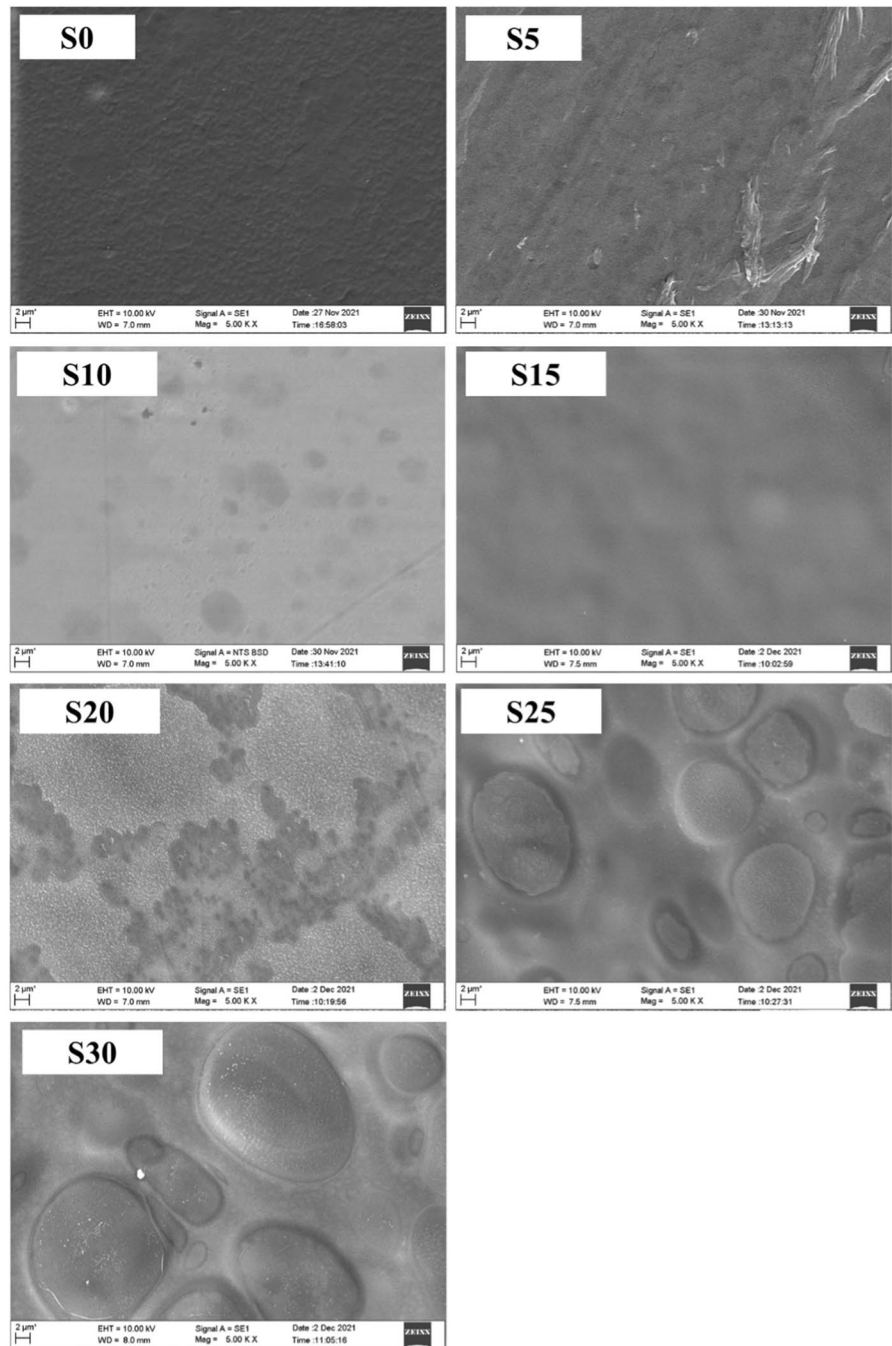
From Fig. 12, it can be seen that the degradation occurs in two steps (El-Sayed et al. 2011; Mazuki

et al. 2019). All the samples show slight mass loss (5 to 25%) for the first decomposition step from 30 to 250 °C. This can be attributed to the loss of humidity that may be absorbed during the sample's handling for testing (Colò et al. 2015). Our results are in-line with what was reported by (Ramesh and Arof 2001; Ahmad and Isa 2016). The second major decomposition step is observed between ~250 °C and 300 °C due to the decomposition of the COO^- group present in the SPE system (Mazuki et al. 2019). The addition of salt is observed to slightly shift the decomposition temperature to a lower temperature, implying a slight decrease in thermal stability. A similar observation was reported by Singh et al. (Singh et al. 2018), who observed a reduction in T_d with the increase in salt concentration. This circumstance may be due to the complexation of the salt with the polymer. Since most energy storage devices are operated at 100 °C or less, our SPE can meet this thermal stability requirement. The major degradation temperature is summarized in Table 6.

Linear sweep voltammetry (LSV) and cyclic voltammetry (CV)

To evaluate the electrochemical stability window (ESW) of the highest conducting polymer electrolyte (S30 sample), LSV has been performed at a scan rate of 5 mV s^{-1} with stainless steel as the working electrode and Na-Hg amalgam as a combined reference and counter electrode. The ESW was approximately 2.63 V (see Fig. 13), which is a good working voltage

Fig. 10 SEM micrographs of NaCMC/PVA-NaI free-standing films



range for sodium batteries. The comparative study of CV on cell Na–Hg|S30|Na–Hg (cell 1) & SS|S30|SS (Cell 2) was performed to confirm the sodium-ion transport in the SPE. The CV trace shows a distinct cathodic and anodic peak for cell-1, while cell-2 does not have such peaks, shown in Fig. 13 inset. Besides, cell-1 has a current magnitude much higher than

cell-2. These findings indicate that cathodic deposition and anodic sodium dissolution at the electrode/electrolyte interface are visible to cell 1. Thus, the transport of Na-ion is confirmed in the prepared SPE (Mishra et al. 2019).

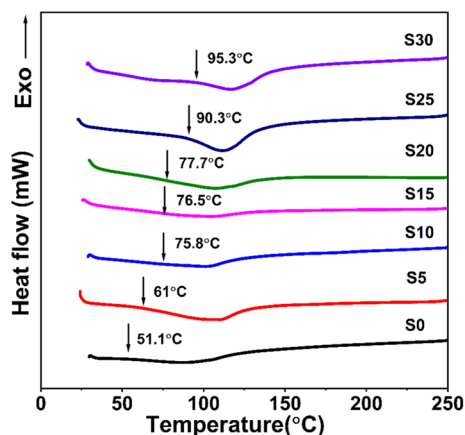


Fig. 11 DSC thermogram of NaCMC/PVA-NaI SPE system

I–t characteristics

The total ionic (t_{ion}) and electronic (t_{elec}) transference number was evaluated using Wagner’s polarization technique. The current is being measured by applying a fixed DC potential of 0.5 V (the applied potential is within the working potential of SPE) to the SS/SPE/SS cell as a function of time. DC biasing leads to the flow of free ions to the oppositely charged electrodes until the cell is completely polarized. Later, residual electronic current flows across the circuit. Thus, the initial current has a contribution of both ions and electrons, whereas the final current is only due to

Fig. 12 TGA thermogram with their respective derivatives, of NaCMC/PVA-NaI SPE system

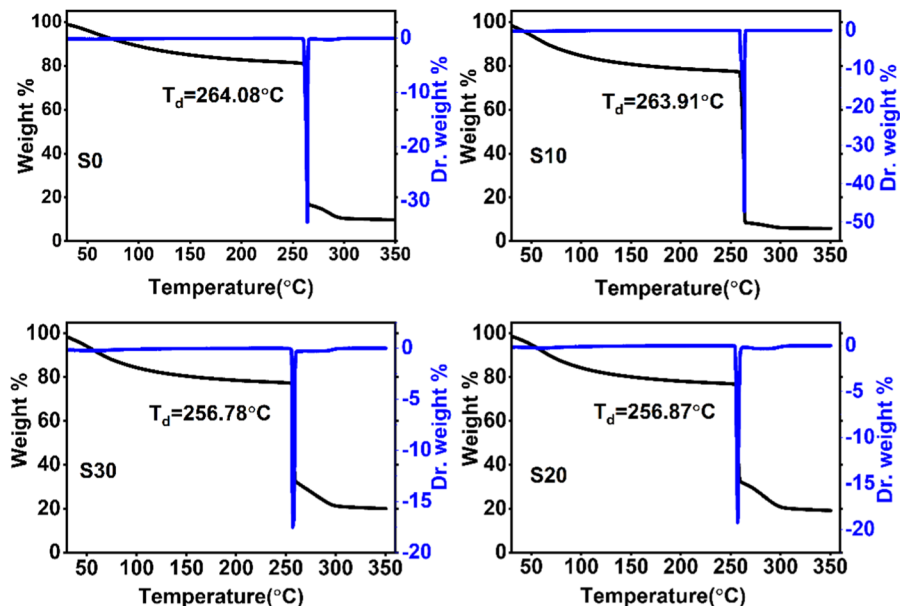


Table 6 Thermal properties of SPEs

Sample	Maximum decomposition temperature (°C)	Maximum decomposition weight loss (%)
S0	264.08	64.24
S10	263.91	68.40
S20	256.87	44.20
S30	256.78	44.10

electrons. The I – t plot of the highest conducting sample (S30 electrolyte) is shown in Fig. 14.

The transference numbers are then calculated from the I – t plot using the equations:

$$t_{ion} = 1 - \frac{I_f}{I_i} \quad (14)$$

$$t_{elec} = 1 - t_{ion} \quad (15)$$

where I_i is the initial current and I_f is the final residual current (Ramesh and Arof 2001). The total ionic transference number was found to be 0.99 for the S30 sample suggesting that the charge transport is predominantly due to ions and not the electrons (Krishna Jyothi et al. 2016).

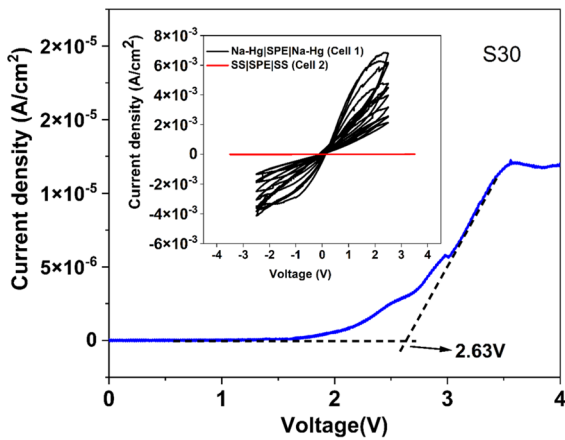


Fig. 13 LSV and comparative CV (inset) plots of sample S30

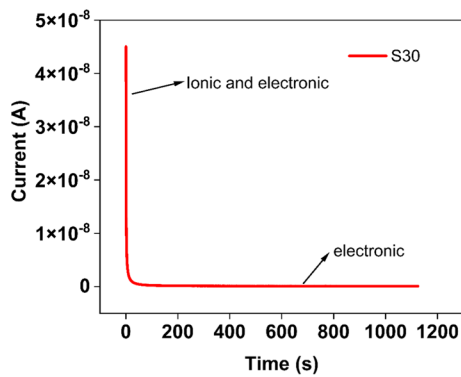


Fig. 14 *I-t* plot of sample S30

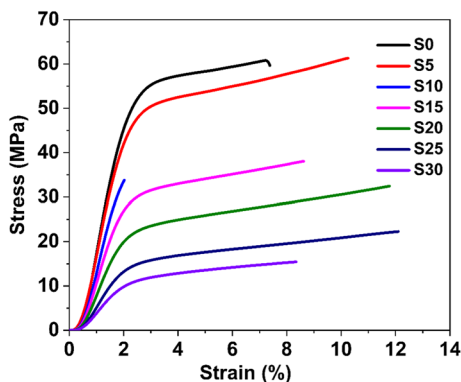


Fig. 15 Stress–strain curves for NaCMC/PVA-NaI SPE system

Table 7 Mechanical properties of NaCMC/PVA-NaI SPE system

Sample	Tensile strength (MPa)	Elongation at break (%)	Youngs modulus (MPa)
S0	60.78	7.40	2467.87
S5	61.29	10.26	2261.00
S10	33.98	2.04	1381.58
S15	38.04	8.63	1461.65
S20	32.46	11.79	1083.89
S25	22.27	12.12	717.70
S30	15.43	8.36	533.34

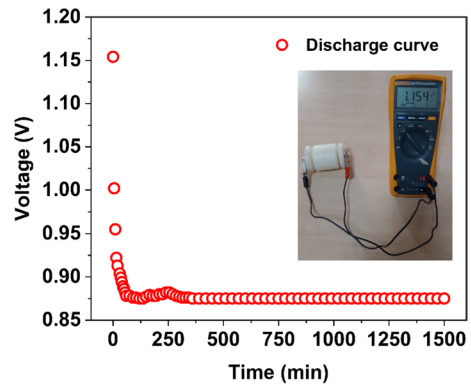


Fig. 16 Discharge profile (monitored for 1 day) of the constructed battery under 100kΩ load along with inset showing the OCV

Mechanical properties

The mechanical properties of the SPE play a critical role in battery performance (Yue et al. 2016). As a result, producing SPE with high ionic conductivity and appropriate mechanical strength at the working temperature is critical. Mechanical properties such as tensile strength, elongation at break, and Young’s modulus were quantified using a stress–strain curve for SPEs. The stress–strain plot for all samples is shown in Fig. 15, and the calculated values are tabulated in Table 7.

Young’s modulus is calculated using the slope of the linear part of the stress–strain curve. The limit of the curve at the stress-plot gives tensile strength and at the strain-axis provides elongation at break. Based on the results shown in Table 7, the softness

Table 8 Cell parameters of the fabricated battery

Specifications of cell parameters (unit)	Dimensions and parameters of cell
Open circuit voltage (V)	1.154
Cell weight (g)	1.120
Cell diameter (mm)	12.000
Cell thickness (mm)	2.377
Cutoff potential (V)	0.875
Current drawn (μ A)	8.750

and flexibility of SPE change with salt concentration and become elastomer (Landel and Nielsen 1993). As the salt concentration increased, the mechanical properties of the SPE reduced. The highest conducting sample (S30 sample) is observed to have the lowest mechanical strength of 15.43 MPa compared to other samples. This may be due to the salt's inhibition of crystallization, leading to the rise in the SPE's amorphousness observed in the XRD analysis (Klongkan and Pumchusak 2015).

Fabrication of solid-state battery

The highest conducting sample has been used as a medium for charge transport in a battery by sandwiching it between anode and cathode in the configuration Zn + ZnSO₄|SPE|V₂O₅ + PbO₅ + SPE + graphite. The photograph of the battery (inset) along with the discharge characteristics under 100 k Ω is shown in Fig. 16.

Initially the battery potential drops from 1.154 to 0.875 V when connected under a 100 k Ω load due to the electrode polarization. The flat region in the discharge curve is called plateau region. The important cell parameters are shown in Table 8.

During the discharge process, oxidation occurs at the anode, and reduction occurs at the cathode. Since H⁺ ions are generated at the anode, it repels off the Na⁺ ions in the polymer electrolyte and eventually reaches the cathode side. We compare the OCV obtained in this study with the previous reports on Na-based electrolytes as given in Table 9. Perhaps with more compatible electrodes, the battery performance can be improved. However, this does not come under the scope of this study.

Conclusions

A new solid polymer electrolyte based on NaCMC/PVA blend polymer doped with different NaI salt concentrations has been prepared by solution casting technique. XRD and FTIR indicate the microstructural changes brought about on the polymer system upon salt doping due to the coordinate bond between Na⁺ cation and the oxygen atom of the –OH functional group of PVA and NaCMC. Sample of 70 wt% NaCMC/PVA-30 wt% NaI (S30 sample) showed the highest amorphous characteristics. An increase in T_g is observed with the addition of salt, which can be attributed to the increase of intermolecular interaction between the Na⁺ cation and the oxygen atom of the polymer chain. Electrical impedance and dielectric analysis reveal an increase in respectively ionic conductivity and dielectric permittivity, owing to an increase in carrier concentration rather than the segmental motion of the polymer chain, suggested by the DSC analysis. The S30 sample showed a high ionic conductivity of 2.52×10^{-3} S cm⁻¹ compared to other doped samples. The mechanical strength for the highest conducting sample is 15.42 MPa, which is the lowest of all the samples measured at room

Table 9 Comparison of OCV of fabricated battery with previous reports

Cell configuration	OCV (V)	Reference
Zn + ZnSO ₄ /film with 1.5 g NaI/PbO ₂ + V ₂ O ₅	0.578	(Subban and Arof 1996)
Zn + ZnSO ₄ /Film with 3.0 g NaClO ₄ /PbO ₂ + V ₂ O ₅	1.121	(Subban et al. 1996)
Zn + ZnSO ₄ ·7H ₂ O/PEO-NaI/0.02 g PbO ₂ + 0.02 g V ₂ O ₅	0.312	(Mohamed et al. 1997)
Zn + ZnSO ₄ ·7H ₂ O /pectin + NaNO ₃ /MnO ₂ + C + pectin + NaNO ₃	0.400	(Vahini et al. 2019)
Zn + ZnSO ₄ ·7H ₂ O NaCMC-PVA-NaI V ₂ O ₅ + PbO ₅ + NaCMC-PVA-NaI + graphite	1.154	Present work

temperature. The total ionic transference number is close to 1, indicating the high ionic nature of the electrolyte.

Acknowledgments Vipin Cyriac acknowledges the Directorate of Minorities, Bengaluru, Government of Karnataka, India for providing financial assistance in the form of *Directorate of Minorities Fellowship for Minority Students*, sanction order: DOM/Fellowship/CR-10/2019-20 dated 29-06-2020. Sincere gratitude to Dr. Sudhakar Y.N of the Department of Chemistry, Manipal Institute of Technology, Manipal, for his valuable comments during this study. The authors thank Z.E. Rojudi of the Physics Department, Faculty of Science, Universiti Putra Malaysia, for carrying out high-temperature dielectric measurements.

Funding Open access funding provided by Manipal Academy of Higher Education, Manipal. The authors have not disclosed any funding.

Declarations

Conflict of interest The authors declare that they have no competing interest.

Human/animal rights The work described in this article did not involve human participants and or animals.

Open Access This article is licensed under a Creative Commons Attribution 4.0 International License, which permits use, sharing, adaptation, distribution and reproduction in any medium or format, as long as you give appropriate credit to the original author(s) and the source, provide a link to the Creative Commons licence, and indicate if changes were made. The images or other third party material in this article are included in the article's Creative Commons licence, unless indicated otherwise in a credit line to the material. If material is not included in the article's Creative Commons licence and your intended use is not permitted by statutory regulation or exceeds the permitted use, you will need to obtain permission directly from the copyright holder. To view a copy of this licence, visit <http://creativecommons.org/licenses/by/4.0/>.

References

- Abd El-Kader FH, Osman WH, Ragab HS et al (2004) Electrical and optical properties of polyvinyl alcohol thin films doped with metal salts. *J Polym Mater* 21:49–60
- Abdullah AM, Aziz SB, Saeed SR (2021) Structural and electrical properties of polyvinyl alcohol (PVA): Methyl cellulose (MC) based solid polymer blend electrolytes inserted with sodium iodide (NaI) salt. *Arab J Chem* 14:103388. <https://doi.org/10.1016/J.ARABJC.2021.103388>
- Ahmad NH, Isa MIN (2016) Characterization of un-plasticized and propylene carbonate plasticized carboxymethyl cellulose doped ammonium chloride solid biopolymer electrolytes. *Carbohydr Polym* 137:426–432
- Arof AK, Amirudin S, Yusof SZ, Noor IM (2014) A method based on impedance spectroscopy to determine transport properties of polymer electrolytes. *Phys Chem Chem Phys* 16:1856–1867
- Aziz SB, Brevik I, Hamsan MH et al (2020) Compatible solid polymer electrolyte based on methyl cellulose for energy storage application: structural, electrical, and electrochemical properties. *Polym* 12:2257. <https://doi.org/10.3390/POLYM12102257>
- Baskaran R, Selvasekarapandian S, Hirankumar G (2004) Bhuvanewari MS (2004) Dielectric and conductivity relaxations in PVAc based polymer electrolytes. *Ionics* 10(10):129–134. <https://doi.org/10.1007/BF02410321>
- Bharati DC, Kumar H, Saroj AL (2020) Chitosan-PEG-NaI based bio-polymer electrolytes: structural, thermal and ion dynamics studies. *Mater Res Express* 6:125360. <https://doi.org/10.1088/2053-1591/AB66A3>
- Bharati DC, Rawat P, Saroj AL (2021) Structural, thermal, and ion dynamics studies of PVA-CS-NaI-based biopolymer electrolyte films. *J Solid State Electrochem* 25:1727–1741. <https://doi.org/10.1007/S10008-021-04946-6/FIGURES/16>
- Bondarenko AS, Ragoisha GA (2005) In: Pomerantsev AL (ed) *Progress in chemometrics research*. Nova Science Publishers, New York, pp 89–102.
- Careem MA, Noor ISM, Arof AK (2020) Impedance spectroscopy in polymer electrolyte characterization. In: Winie T, Arof AK, Thomas S (eds) *Polymer electrolytes*. Wiley, New York, pp 23–64. <https://doi.org/10.1002/9783527805457.ch2>
- Chai KL, Noor IM, Aung MM et al (2020) Non-edible oil based polyurethane acrylate with tetrabutylammonium iodide gel polymer electrolytes for dye-sensitized solar cells. *Sol Energy* 208:457–468. <https://doi.org/10.1016/J.SOLENER.2020.08.020>
- Chitra R, Sathya P, Selvasekarapandian S et al (2019) Synthesis and characterization of iota-carrageenan solid biopolymer electrolytes for electrochemical applications. *Ionics (kiel)* 25:2147–2157. <https://doi.org/10.1007/s11581-018-2687-z>
- Colò F, Bella F, Nair JR et al (2015) Cellulose-based novel hybrid polymer electrolytes for green and efficient Na-ion batteries. *Electrochim Acta* 174:185–190. <https://doi.org/10.1016/j.electacta.2015.05.178>
- De Melo EM, Clark JH, Matharu AS (2017) The Hy-MASS concept: Hydrothermal microwave assisted selective scissoring of cellulose for: In situ production of (meso)porous nanocellulose fibrils and crystals. *Green Chem* 19:3408–3417. <https://doi.org/10.1039/c7gc01378g>
- del Cerro DR, Koso TV, Kakko T et al (2020) Crystallinity reduction and enhancement in the chemical reactivity of cellulose by non-dissolving pre-treatment with tetrabutylphosphonium acetate. *Cellul* 2710(27):5545–5562. <https://doi.org/10.1007/S10570-020-03044-6>
- El-Sayed S, Mahmoud KH, Fatah AA, Hassen A (2011) DSC, TGA and dielectric properties of carboxymethyl cellulose/polyvinyl alcohol blends. *Phys B Condens Matter* 406:4068–4076. <https://doi.org/10.1016/j.physb.2011.07.050>

- Fergus JW (2010) Ceramic and polymeric solid electrolytes for lithium-ion batteries. *J Power Sources* 195:4554–4569. <https://doi.org/10.1016/J.JPOWSOUR.2010.01.076>
- French AD (2013) (2013) Idealized powder diffraction patterns for cellulose polymorphs. *Cellul* 212(21):885–896. <https://doi.org/10.1007/S10570-013-0030-4>
- Furtado CA, Silva GG, Machado JC, Pimenta MA, Silva RA (1999) Study of correlations between microstructure and conductivity in a thermoplastic polyurethane electrolyte. *J Phys Chem B* 103(34):7102–7110
- He R, Kyu T (2016) Effect of plasticization on ionic conductivity enhancement in relation to glass transition temperature of crosslinked polymer electrolyte membranes. *Macromolecules* 49:5637–5648
- Hodge RM, Edward GH, Simon GP (1996) Water absorption and states of water in semicrystalline poly(vinyl alcohol) films. *Polymer (guildf)* 37:1371–1376. [https://doi.org/10.1016/0032-3861\(96\)81134-7](https://doi.org/10.1016/0032-3861(96)81134-7)
- Jiang C, Li H, Wang C (2017) Recent progress in solid-state electrolytes for alkali-ion batteries. *Sci Bull* 62:1473–1490. <https://doi.org/10.1016/j.scib.2017.10.011>
- Jonscher AK (1999) Dielectric relaxation in solids. *J Phys D Appl Phys* 32:R57. <https://doi.org/10.1088/0022-3727/32/14/201>
- Khoramabadi HN, Arefian M, Hojjati M et al (2020) A review of Polyvinyl alcohol/Carboxymethyl cellulose (PVA/CMC) composites for various applications. *J Compos Compd* 2:69–76
- Klongkan S, Pumchusak J (2015) Effects of the addition of LiCF₃SO₃ Salt on the conductivity, thermal and mechanical properties of PEO-LiCF₃SO₃ solid polymer electrolyte. *Int J Chem Eng Appl* 6:165–168. <https://doi.org/10.7763/ijcea.2015.v6.474>
- Krishna Jyothi N, Vijaya Kumar K, Sunita Sundari G, Narayana Murthy P (2016) Ionic conductivity and battery characteristic studies of a new PAN-based Na⁺ ion conducting gel polymer electrolyte system. *Indian J Phys* 90:289–296. <https://doi.org/10.1007/s12648-015-0758-9>
- Kumar M, Tiwari T, Chauhan JK, Srivastava N (2014) Understanding the ion dynamics and relaxation behavior from impedance spectroscopy of NaI doped Zwitterionic polymer system. *Mater Res Express* 1:045003. <https://doi.org/10.1088/2053-1591/1/4/045003>
- Landel RF, Nielsen LE (1993) Mechanical properties of polymers and composites. CRC Press, Boca Raton
- Li X-F, Li F, Shi Y et al (2005) Nature of proton dynamics in a polymer electrolyte membrane, nafion: a first-principles molecular dynamics study. *Solid State Ionics* 176:3673–3680. <https://doi.org/10.1063/1.2192777>
- MacGlashan GS, Andreev YG, Bruce PG (1999) Structure of the polymer electrolyte poly(ethylene oxide):6:LiAsF₆. *Nature* 398:792–794. <https://doi.org/10.1038/19730>
- Mazuki NF, Rasali NMJ, Saadiah MA, Samsudin AS (2018) Irregularities trend in electrical conductivity of CMC/PVA-NH₄Cl based solid biopolymer electrolytes. *AIP Conf Proc* 2030:020221. <https://doi.org/10.1063/1.50666862>
- Mazuki NF, Fuzlin AF, Saadiah MA, Samsudin AS (2019) An investigation on the abnormal trend of the conductivity properties of CMC/PVA-doped NH₄Cl-based solid biopolymer electrolyte system. *Ionics (kiel)* 25:2657–2667. <https://doi.org/10.1007/s11581-018-2734-9>
- Mishra K, Arif T, Kumar R, Kumar D (2019) Effect of Al₂O₃ nanoparticles on ionic conductivity of PVdF-HFP/PMMA blend-based Na⁺-ion conducting nanocomposite gel polymer electrolyte. *J Solid State Electrochem* 23:2401–2409. <https://doi.org/10.1007/s10008-019-04348-9>
- Mohamed NS, Zakaria MZ, Ali AMM, Arof AK (1997) Characteristics of poly(ethylene oxide)-NaI polymer electrolyte and electrochemical cell performances. *J Power Sources* 66:169–172. [https://doi.org/10.1016/S0378-7753\(96\)02541-4](https://doi.org/10.1016/S0378-7753(96)02541-4)
- Mohd Ali NS, Nagao Y, Samsudin AS (2020) Ethylene carbonate and polyethylene glycol as efficient plasticizers in CMC-PVA-NH₄NO₃-based polymer electrolyte. *Makara J Technol* 24(1):13
- Muthuvinnayagam M, Gopinathan C (2015) Characterization of proton conducting polymer blend electrolytes based on PVdF-PVA. *Polymer (guildf)* 68:122–130. <https://doi.org/10.1016/J.POLYMER.2015.05.008>
- Ngai KS, Ramesh S, Ramesh K, Juan JC (2016) A review of polymer electrolytes: fundamental, approaches and applications. *Ionics (kiel)* 22:1259–1279. <https://doi.org/10.1007/s11581-016-1756-4>
- Noor I (2020) Determination of charge carrier transport properties of gellan gum–lithium triflate solid polymer electrolyte from vibrational spectroscopy. *High Perform Polym* 32:168–174. <https://doi.org/10.1177/0954008319890016>
- Noor NAM, Isa MIN (2019) Investigation on transport and thermal studies of solid polymer electrolyte based on carboxymethyl cellulose doped ammonium thiocyanate for potential application in electrochemical devices. *Int J Hydrogen Energy* 44:8298–8306
- Noor IS, Majid SR, Arof AK (2013) Poly(vinyl alcohol)–LiBOB complexes for lithium–air cells. *Electrochim Acta* 102:149–160. <https://doi.org/10.1016/J.ELECTACTA.2013.04.010>
- Pawlicka A, Danczuk M, Wiczorek W, Zygadlo-Monikowska E (2008) Influence of plasticizer type on the properties of polymer electrolytes based on Chitosan⁺. *J Phys Chem A* 112:8888–8895. <https://doi.org/10.1021/JP801573H>
- Pritam AA, Sharma AL (2020) Selection of best composition of Na⁺ ion conducting PEO-PEI blend solid polymer electrolyte based on structural, electrical, and dielectric spectroscopic analysis. *Ionics (kiel)* 26:745–766. <https://doi.org/10.1007/s11581-019-03245-5>
- Pritam Arya A, Sharma AL (2021) Conductivity and dielectric spectroscopy of Na⁺ ion conducting blended solid polymer nanocomposites. In: Sharma Yogesh, Varma Ghanshyam Das, Mukhopadhyay Amartya, Thangadurai Venkataraman (eds) Recent research trends in energy storage devices. Springer, Singapore
- Ramesh S, Arof AK (2001) Structural, thermal and electrochemical cell characteristics of poly(vinyl chloride)-based polymer electrolytes. *J Power Sources* 99:41–47. [https://doi.org/10.1016/S0378-7753\(00\)00690-X](https://doi.org/10.1016/S0378-7753(00)00690-X)
- Ramlli MA, Isa MIN (2016) Structural and ionic transport properties of protonic conducting solid biopolymer electrolytes based on carboxymethyl cellulose doped with ammonium fluoride. *J Phys Chem B* 120:11567–11573. <https://doi.org/10.1021/acs.jpcc.6b06068>
- Rani NS, Sannappa J, Demappa T (2014a) Structural, thermal, and electrical studies of sodium iodide (NaI)-doped hydroxypropyl methylcellulose (HPMC) polymer

- electrolyte films. *Ionics (kiel)* 20:201–207. <https://doi.org/10.1007/S11581-013-0952-8/TABLES/4>
- Rani NS, Sannappa J, Demappa T (2014b) Effects of CdCl₂ concentration on the structural, thermal and ionic conductivity properties of HPMC polymer electrolyte films. *Ionics* 211(21):133–140. <https://doi.org/10.1007/S11581-014-1151-Y>
- Saadiah MA, Zhang D, Nagao Y et al (2019) Reducing crystallinity on thin film based CMC/PVA hybrid polymer for application as a host in polymer electrolytes. *J Non Cryst Solids* 511:201–211. <https://doi.org/10.1016/j.jnoncrsol.2018.11.032>
- Saadiah MA, Nagao Y, Samsudin AS (2020) Proton (H⁺) transport properties of CMC–PVA blended polymer solid electrolyte doped with NH₄NO₃. *Int J Hydrogen Energy* 45:14880–14896
- Saidi NM, Ming Ng H, Omar FS et al (2019) Polyacrylonitrile–poly(1-vinyl pyrrolidone-co-vinyl acetate) blend based gel polymer electrolytes incorporated with sodium iodide salt for dye-sensitized solar cell applications. *J Appl Polym Sci* 136:47810. <https://doi.org/10.1002/APP.47810>
- Saminatha Kumaran V, Ng HM, Ramesh S et al (2018) The conductivity and dielectric studies of solid polymer electrolytes based on poly (acrylamide-co-acrylic acid) doped with sodium iodide. *Ionics (kiel)* 24:1947–1953. <https://doi.org/10.1007/S11581-018-2448-Z/FIGURES/5>
- Selvanathan V, Halim MNA, Azzahari AD et al (2018) Effect of polar aprotic solvents on hydroxyethyl cellulose-based gel polymer electrolyte. *Ionics* 247(24):1955–1964. <https://doi.org/10.1007/S11581-018-2455-0>
- Shanmuga Priya S, Karthika M, Selvasekarapandian S, Manjuladevi R (2018) Preparation and characterization of polymer electrolyte based on biopolymer I-Carrageenan with magnesium nitrate. *Solid State Ionics* 327:136–149. <https://doi.org/10.1016/J.SSI.2018.10.031>
- Shetty SK, Ismayil HS et al (2021a) Dielectric relaxations and ion transport study of NaCMC:NaNO₃ solid polymer electrolyte films. *Ionics (kiel)* 27:2509–2525. <https://doi.org/10.1007/s11581-021-04023-y>
- Shetty SK, Ismayil Nasreen, Swathi Mahesha MG, Rashmitha K (2021b) Sodium ion conducting PVA/NaCMC bio poly-blend electrolyte films for energy storage device applications. *International Journal of Polymer Analysis and Characterization* 26:411–424. <https://doi.org/10.1080/1023666X.2021.1899685>
- Singh R, Polu AR, Bhattacharya B et al (2016) Perspectives for solid biopolymer electrolytes in dye sensitized solar cell and battery application. *Renew Sustain Energy Rev* 65:1098–1117. <https://doi.org/10.1016/J.RSER.2016.06.026>
- Singh P, Bharati DC, Gupta PN, Saroj AL (2018) Vibrational, thermal and ion transport properties of PVA-PVP-PEG-MeSO₄Na based polymer blend electrolyte films. *J Non Cryst Solids* 494:21–30. <https://doi.org/10.1016/j.jnoncrsol.2018.04.052>
- Singh P, Gupta PN, Saroj AL (2020) Ion dynamics and dielectric relaxation behavior of PVA-PVP-NaI-SiO₂ based nano-composites polymer blend electrolytes. *Phys B Condens Matter* 578:411850. <https://doi.org/10.1016/J.PHYSB.2019.411850>
- Steiner T (2002) The hydrogen bond in the solid state. *Angew Chem Int Ed Engl* 41:49–76
- Su'ait MS, Ahmad A, Hamzah H, Rahman MYA (2011) Effect of lithium salt concentrations on blended 49% poly(methyl methacrylate) grafted natural rubber and poly(methyl methacrylate) based solid polymer electrolyte. *Electrochim Acta* 57:123–131. <https://doi.org/10.1016/J.ELECTACTA.2011.06.015>
- Subban RHY, Arof AK (1996) Sodium iodide added chitosan electrolyte film for polymer batteries. *Phys Scr* 53:382. <https://doi.org/10.1088/0031-8949/53/3/021>
- Subban RHY, Arof AK, Radhakrishna S (1996) Polymer batteries with chitosan electrolyte mixed with sodium perchlorate. *Mater Sci Eng B* 38:156–160. [https://doi.org/10.1016/0921-5107\(95\)01508-6](https://doi.org/10.1016/0921-5107(95)01508-6)
- Tang R, Jiang C, Qian W et al (2015) Dielectric relaxation, resonance and scaling behaviors in Sr₃Co₂Fe₂₄O₄₁ hexaferrite. *Sci Rep* 5:1–11. <https://doi.org/10.1038/srep13645>
- Tellamekala S, Ojha P, Gopal NO et al (2020) Effect of K⁺ ion doping on structural and physical properties of PVA/MAA:EA polymer blend electrolytes. *Mater Res Innov* 25:287–299
- Vahini M, Muthuvinayagam M, Isa MIN (2019) Preparation and characterization of biopolymer electrolytes based on pectin and NaNO₃ for battery applications. *Polym Sci Ser A* 61:823–831. <https://doi.org/10.1134/S0965545X19060129>
- Wang K, Ju S, Gao Q et al (2021) Porous sulfurized poly(acrylonitrile) nanofiber as a long-life and high-capacity cathode for lithium–sulfur batteries. *J Alloys Compd* 860:158445. <https://doi.org/10.1016/J.JALLCOM.2020.158445>
- Wojdyr M, Gierlotka S, Palosz B (2004) FITYK – peak-fitting software with support for powder patterns analysis. *Acta Crystallogr Sect A Found Crystallogr* 60:s246–s246. <https://doi.org/10.1107/S010876730409511X>
- Yadav M, Kumar M, Tiwari T, Srivastava N (2017) Wheat starch + NaI: a high conducting environment friendly electrolyte system for energy devices. *Ionics (kiel)* 23:2871–2880. <https://doi.org/10.1007/s11581-016-1930-8>
- Yao W, Weng Y, Catchmark JM (2020) Improved cellulose X-ray diffraction analysis using Fourier series modeling. *Cellul* 27:5563–5579. <https://doi.org/10.1007/S10570-020-03177-8>
- Yue L, Ma J, Zhang J et al (2016) All solid-state polymer electrolytes for high-performance lithium ion batteries. Elsevier, Amsterdam
- Zhang X, Daigle J-C, Zaghib K (2020) Comprehensive review of polymer architecture for all-solid-state lithium rechargeable batteries. *Mater* 13:2488. <https://doi.org/10.3390/MA13124888>
- Zulkifli A, Saadiah MA, Mazuki NF, Samsudin AS (2020) Characterization of an amorphous materials hybrid polymer electrolyte based on a LiNO₃-doped, CMC-PVA blend for application in an electrical double layer capacitor. *Mater Chem Phys* 253:123312. <https://doi.org/10.1016/j.matchemphys.2020.123312>

Publisher's Note Springer Nature remains neutral with regard to jurisdictional claims in published maps and institutional affiliations.